## **PAPER • OPEN ACCESS**

# Simultaneous irradiation and thermal effects on 16 MeV proton irradiated tungsten samples

To cite this article: R Rayaprolu et al 2021 Phys. Scr. 96 124014

View the <u>article online</u> for updates and enhancements.

# Physica Scripta



#### **OPEN ACCESS**

#### RECEIVED

1 June 2021

#### REVISED

4 August 2021

ACCEPTED FOR PUBLICATION

12 August 2021

#### PUBLISHED

30 August 2021

Original content from this work may be used under the terms of the Creative Commons Attribution 4.0 licence.

Any further distribution of this work must maintain attribution to the author(s) and the title of the work, journal citation and DOL



#### **PAPER**

# Simultaneous irradiation and thermal effects on 16 MeV proton irradiated tungsten samples

R Rayaprolu<sup>1</sup>, S Möller<sup>1</sup>, I Spahn<sup>2</sup>, D Höschen<sup>1</sup> and Ch Linsmeier<sup>1</sup>

- <sup>1</sup> Forschungszentrum Jülich GmbH, Institut für Energie- und Klimaforschung—Plasma physik, 52425 Jülich, Germany
- <sup>2</sup> Forschungszentrum Jülich GmbH, Institut für Neurowissenschaften und Medizin -Nuklearchemie, 52425 Jülich, Germany

E-mail: r.rayaprolu@fz-juelich.de

Keywords: tungsten, fusion, neutron irradiation, proton irradiation, hardness, transmutation

#### Abstract

16 MeV protons have been used to irradiate 300  $\mu$ m thick macroscopic W samples in a pilot experiment to 0.006 dpa damage dose under low and high temperature scenarios of ~373 K and ~1223 K, respectively. The linear pre-Bragg region has been used for damage where the electronic loss (heat) in the sample amounts to 1.5 MW  $\cdot$  m<sup>-2</sup>. Post high-temperature irradiation, the W sample has been recrystallized as seen under the scanning electron microscope. Indentation measurements on the surface show a softening of 0.6 GPa post-recrystallization against an irradiation hardening of 0.8 GPa for the low-temperature irradiation scenario.

#### 1. Introduction

Nuclear fusion reactors are designed to maximize high energy deuterium and tritium ion collisions within a confined magnetic field. The fusion reactor inner walls are the first point of contact for errant ions, neutralised energetic particles and high energy neutrons. The inner wall is subjected to plasma impingement of  $10^{21} \, \text{m}^{-2} \text{s}^{-1}$ , heat fluxes between 1-10 MW  $\cdot$  m<sup>-2</sup> and neutron fluxes of  $10^{19} \, \text{m}^{-2} \text{s}^{-1}$  [1–3]. Hence, understanding the combined influence of plasma, heat loads and neutron damage is essential in the selection of plasma-facing materials.

The influence of fusion neutron damage is not completely understood, let alone combined damage. Ions are often used to recreate and accelerate radiation damage in materials. Heavy ion accelerator experiments, focus on concentrating large damages within a narrow width ( $\sim 1 \mu m$ ) of the Bragg peak to probe neutron damage [4–7]. This damage is additionally devoid of nuclear transmutation reactions. However, heavy-ion irradiation damage morphology is compact-large clusters of damage, and the cluster size is thought to be similar to neutron irradiation damage. Proton irradiation studies have also been used to mimic various aspects of neutron damage [8]. Conventionally these have been performed using low energy protons up to 5MeV energy, and the emphasis has still been to use the Bragg peak accumulated damage. While the damage cluster size produced by low energy proton irradiation is smaller as compared to heavy-ion damage, the damage clusters are spaced further apart, similar to neutron interactions [9]. Another approach, which is followed in this work, is based on the use of the linear pre-Bragg damage region, as previously described in [10]. Using higher energy protons (12–30MeV), as shown in figure 1 for 16 and 30 MeV protons on tungsten(W), the range of proton damage in the plateau region prior to the Bragg peak is over 300  $\mu$ m and can be used to investigate macroscopic properties. Additionally, at higher energies, protons can induce transmutational reactions [11, 12]. This makes the method complementary to fission reactor studies. Combining the range of uniform pre-Bragg damage with a maximum  $5 \times \text{limit}$  on the variation in transmutation as explained in [11], the sample thickness for the corresponding proton energy is established. Limiting the sample thickness to the linear pre-Bragg regime also mitigates implantation of protons/hydrogen within the sample. Furthermore, at higher proton energies, head-on collisions with simple Coulomb interaction increases in probability, thus additionally allowing the production of high energy recoils [9].

Furthermore, the pre-Bragg region realises energy transfer from the stopping of protons to the electrons. This induces an additional simultaneous heat load on the sample. While the heat is deposited within the sample,

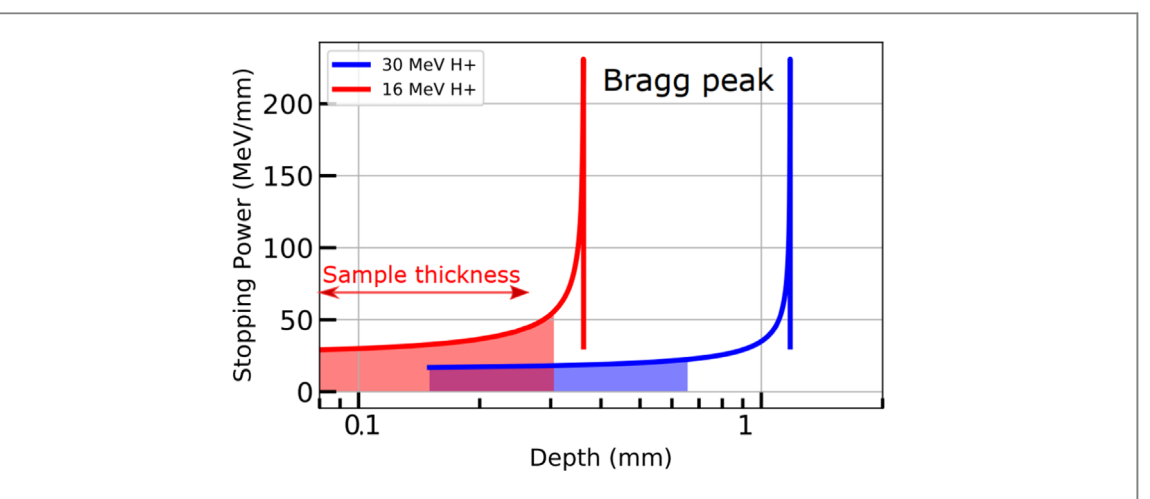


**Figure 1.** Loss of energy for charged particles with the linear pre Bragg damage region highlighted, calculated using SRIM [13]. The Bragg peak has a high damage rate within a very concentrated region, while the linear pre-Bragg region has a low damage rate over a longer damage width.

the 1-dimensional nature of conduction occurring within the sample body can be suitably modelled as virtual heat flux and particle flux on the surface of the sample. High current (  $\sim \mu$  A) and energies of  $10\times$  MeV on mm-sized samples would result in a heat flux of MW  $\cdot$  m  $^{-2}$  level, which is a close approximation to the value of the fusion conditions. W is often cold worked to induce ductility through microstructure [14]. At high temperatures, recovery is seen in W, which leads to recrystallization at higher temperatures and longer times. However, upon recrystallization, W shows embrittlement, and inter-granular cracks [15]. The embrittlement is further enhanced by irradiation and a combined radiation under high heat flux is essential to material property selection. The higher energy proton irradiation is capable of inflicting high heat fluxes and simultaneously induce irradiation damage. These irradiations aim to quantify engineering properties under fusion relevant irradiation conditions.

This contribution describes the accelerator irradiation technique in a pilot irradiation. The sample preparation and holder arrangement are initially explained, alongside irradiation temperature control through contact and cooling. Post-irradiation, first results from a high temperature operation scenario are subsequently detailed with nuclear transmutation quantification, microscopy and hardness measurements.

### 2. Sample design and setup for proton irradiation

The possibility of sample miniaturization to reduce radiation exposure to personnel and machine has been previously investigated for fission reactors [16–19]. In order to have easy inter-changeability and compare values between fission and proton irradiation, the proton samples were designed conforming to the above recommendations. In accelerators, the beam size and volume often varies between 6–12 mm in diameter and induces further space constraints [20]. To suitably comply, a nominal sample diameter of 12 mm with 10 mm active size is considered towards compatibility within most accelerators. Additionally, from the perspective of post-irradiation testing, the sample is designed to incorporate specially developed testing techniques for macroscopic yet miniaturized samples; tensile testing, punch testing and instrumented indentation. Thus, the sample has a tensile stub in the centre with four surrounding disks of 3 mm diameter (TEM disks) as shown in figure 2. The multiple 3 mm disks add redundancy to the irradiation and testing. The sample is cut using electrodischarge machining and then polished up to 1  $\mu$ m grain size.

The sample is loaded onto a water-cooled copper sample holder. Heat removal from the sample occurs through conduction, and a proper physical contact is required between the sample and the holder. To facilitate this, a copper disk with precise grooves for the tensile and 3 mm disks is placed over the W sample as shown in figure 3. A copper nut is then screwed on to lock the sample in position and press the copper disk down onto the W sample and ensure thermal contact. Additional modifications were carried out to incorporate *in situ* temperature measurement. Three 0.5 mm diameter holes were drilled through the copper sample holder to incorporate three thermocouples, as shown in figure 3. These thermocouples are also locked into position through the use of a spring.

The thermocouples are type N with Inconel600 as the sheath material and having an operating regime between 73 K to 1423 K. They are in contact with the backside surface of the sample and measure the temperature *in situ* during irradiation. The initial temperature pre-irradiation is recorded as 285 K. Once



**Figure 2.** Sample designed for higher energy proton irradiation with a 10 mm active diameter. Each sample consists of one tensile sample with four 3 mm disks arranged around the tensile sample.

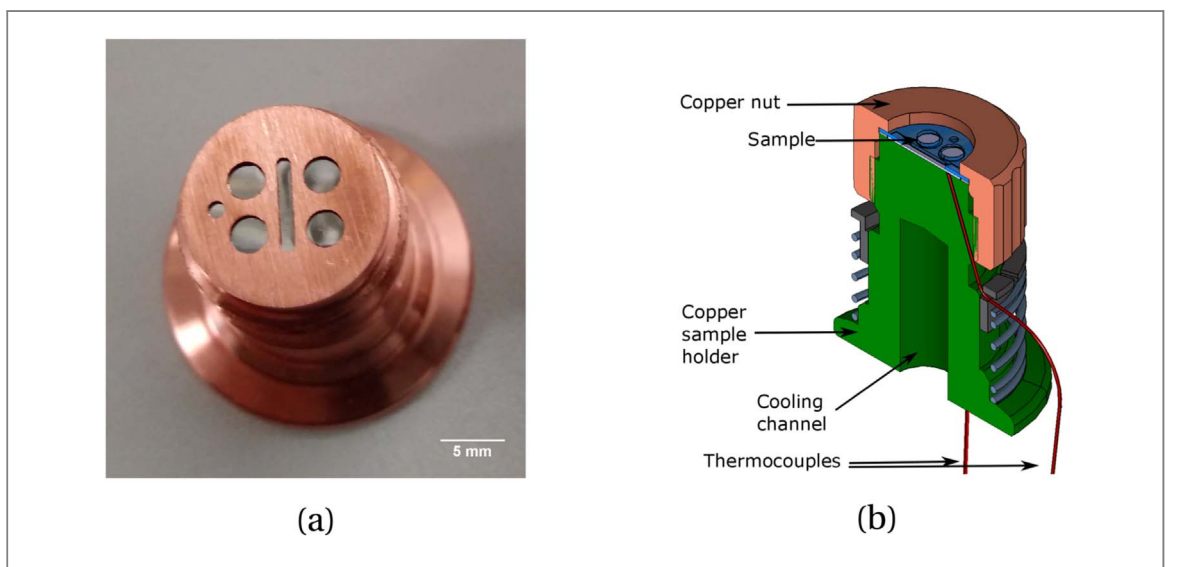


**Figure 3.** Sample holder design and assembly. (a) Polished W sample in a Cu sample holder pressed with a Cu disk for thermal contact. (b) Model sketch slice of the assembled sample holder displaying the thermocouples, cooling water channel and the sample holder.

irradiation starts, a rapid increase in temperature is noted, stabilising at  $373 \pm 5$  K. Keeping the heat flux constant, and by changing the surface contact between the sample and the copper sample holder, the irradiation temperatures can be changed. Two different contact scenarios; full-sample contact or low-temperature irradiation scenario and outer-edge contact or high-temperature scenario are investigated and explained in the next section.

#### 3. 16 MeV proton irradiation

A pilot irradiation to demonstrate the two operation scenarios; full-contact or low-temperature irradiation and outer-edge contact or high-temperature irradiation as shown in figure 4 is carried out on the Baby cyclotron [21] using 16.5 MeV protons on a 300  $\mu$ m thick W sample. The irradiation is performed at 10  $\mu$ A current and a beam diameter of 10 mm. SRIM estimates that 99.9% of the protons exit the sample with an energy of ~4.6 MeV; thus undergoing an electronic stopping loss of 12 MeV per proton within the 300  $\mu$ m range. This results in a heat flux of ~1.5 MW · m<sup>-2</sup>  $\left(\frac{12 \text{ MeV} \times 10 \ \mu\text{A}}{\pi 5^2}\right)$  as per equation (1), where E is the energy loss per proton in MeV and I is the proton current in  $\mu$ A and S is the proton irradiated area (spot size) in mm<sup>2</sup>.

$$Q = \frac{E \times I}{S} \tag{1}$$

Initially, the sample is irradiated at the low-temperature scenario for two hours (20  $\mu$ A · hours) after which it is readjusted in the sample holder for a high-temperature irradiation to a total of 40  $\mu$ A · hours. The damage calculation is performed using the quick calculation setup on SRIM [13] with a displacement damage threshold of 90eV [22] in accordance to the technique prescribed by Stoller *et al* [23]. However, as the range is restricted to

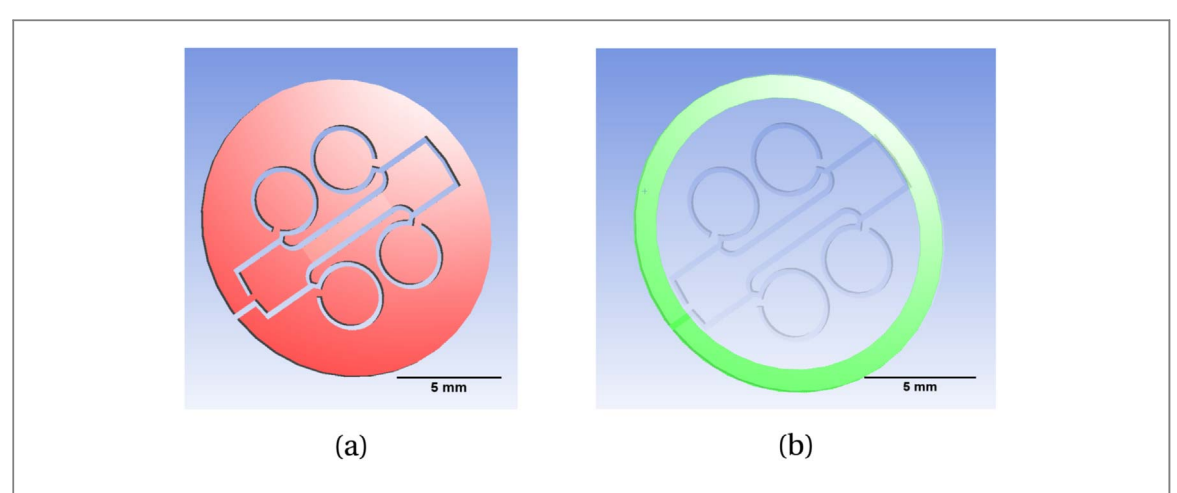


**Figure 4.** The contact scenario between the sample and the holder induces the range of irradiation temperatures. (a) Low temperature irradiation scenario with full backside sample surface contact. (b) High temperature irradiation scenario- only sample outer-edge contact.

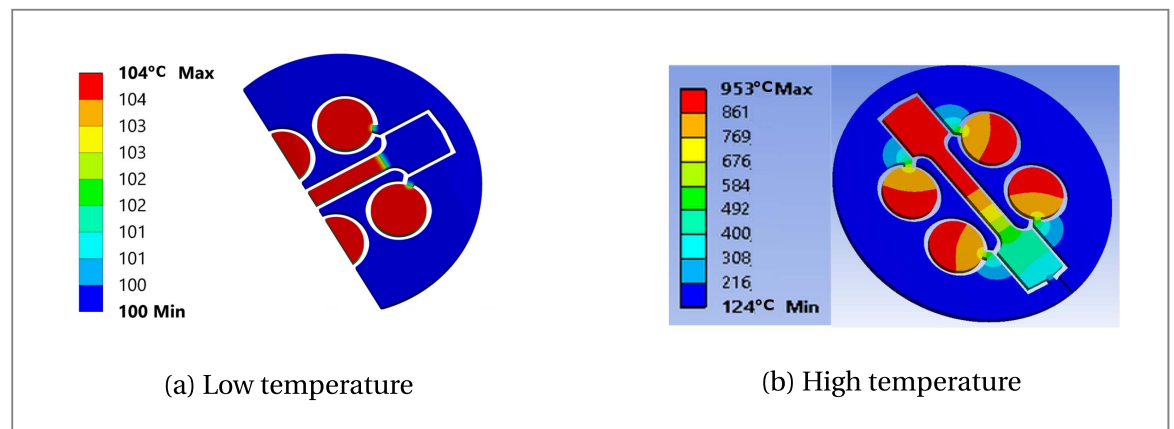


Figure 5. Irradiation temperature simulated using steady state thermal analysis mode in ANSYS19.1 displaying the low temperature and high temperature irradiations.

300  $\mu$ m, internal target vacancies from SRIM are substituted for displacements per ion (DPI) in equation (2). For an atomic material density  $\rho$ , the proton current I projected on spot size S in range R as per equation (2) provides the damage dose rate DPA(t) [10]. This corresponds to a dose rate of  $4.3 \times 10^{-7}$  dpa · s<sup>-1</sup> culminating in a damage dose of 0.006 dpa. During the low-temperature scenario, the thermocouples displayed a constant temperature of 373 K. A second sample is additionally irradiated at 1  $\mu$ A current (no significant thermal loads) to a similar dose of 0.007 dpa in order to study the effects of pure irradiation hardening using 16 MeV protons. Both samples are irradiated under a minimum vacuum pressure of  $5 \times 10^{-2}$  mbar to avoid oxidation effects.

$$DPA(t) = \frac{I}{R\rho S} \times DPI \tag{2}$$

Thermocouple readings and the heat deposition are used in a steady-state thermal ANSYS19.1 simulation to determine the exact irradiation temperature as shown in figure 5. As the sample is thin, with good thermal contact the sample temperature is not expected to change significantly as shown by ANSYS and the low-temperature irradiation scenario maximum temperature is 377 K. This is the minimum temperature at which irradiation can be carried out at 10  $\mu$ A proton current on W. During the high-temperature irradiation, only the outer edge contact is enforced. Here a proper contact to the thermocouple is possible only at the outer edge and not directly at the sample. This is used as an input in ANSYS and the high-temperature scenario describes the maximum irradiation temperature at 1226 K. The tensile sample portion, which is furthest from connection to the main body, is seen to be at the maximum temperature.

**Table 1.** Comparison of FISPACT-II simulated activity with gamma ray analysis measurement activity

Nuclide Simul	lated (Bq) Measured (Bq)
<sup>184</sup> mRe 1.9 <sup>183</sup> Re 1.0	$\begin{array}{ccc} 2 \times 10^6 & 8.05 \pm 0.2 \times 10^5 \\ 6 \times 10^5 & 8.79 \pm 0.3 \times 10^4 \\ 3 \times 10^7 & 9.22 \pm 0.3 \times 10^5 \\ 99.1 & 3.38 \pm 0.1 \times 10^3 \end{array}$

# 4. Post irradiation analysis

Rhenium(Re) is a transmutation product and is seen to precipitate out in fission reactor studies, leading to irradiation hardening [24-27]. However, fission reactors have a thermal neutron peaked spectrum compared to the high energy shifted spectrum in fusion reactors. The large thermal neutron capture cross-section leads to an overproduction of Re through  $(n, \gamma)$  transmutation compared to a fusion irradiation scenario. 16–30 MeV proton irradiation simulations using FISPACT-II suggest a closer fusion relevant Re transmutation rate. Postirradiation, the sample radioactivity is measured using an energy and efficiency calibrated HPGe detector of 30% efficiency. The sample placed 80 cm away from the detector is counted for a total live time of 86 400 seconds. The cooling time post-irradiation is suitably adjusted to reflect the measured activity. A comparison with combined MCNP6.1 [28] and FISPACT-II [29] simulated activity calculations using TENDL-2015 cross-sections [30] is shown in table 1. The results in table 1 indicate a good agreement within  $2 \times$  for the  $^{184}$ Re isotopes, while there is a higher discrepancy for <sup>183</sup>Re. This discrepancy is due to the use of computed cross-sections in the absence of experimental cross-sections. There has been a correction in the updated version TENDL computed crosssections. On average, the <sup>184</sup>W (p,n) <sup>183</sup>Re cross-section in the later versions TENDL-2017 and TENDL-2019are  $0.1 \times$  of the 2015 data, which accounts for the discrepancy in  $^{183}$ Re production and if corrected, also agrees with the measured activity within 2×of predicted activity. Correspondingly, the measured dose rate 4.3 mSv/hr, is  $3.5 \times$  lower than the simulated dose rate of 14.7 mSv/hr. Such an outcome of over prediction of dose rates ensures a degree of safety with the radioactive sample.

Scanning electron microscopy of the sample performed after high-temperature irradiation shows a drastic change on the sample surface. Figure 6 shows a comparison of the unirradiated (pristine) sample (a) & (b), with the irradiated (0.006 dpa) surface (e) & (f) and the copper casing protected surface (0 dpa)(c) & (d), at similar magnifications of 100× and 1000× under the scanning electron microscope. The pristine picture represents a clean sample with grains seen on the surface. They are clearly visible at the higher magnification of  $1000 \times$ . Part of the sample lies below the copper casing and is not subject to direct proton exposure. However, heat transfer takes place from the copper disk through the sample and results in a change in microstructure. A roughening of the surface is noticed, and under 1000×magnification, a heat-affected surface is seen. The sample, which is under direct proton irradiation and the heat flux, shows the onset of the recrystallization of the sample. Similar observations have been made, albeit under much higher heat fluxes of  $10 \& 20 \,\mathrm{MW} \cdot \mathrm{m}^{-2}$  [31]. A recrystallization post neutron irradiation at a similar irradiation temperature of 1223 K at HFIR is reported, however at a higher irradiation dose of 0.7dpa corresponding to 94 days [32]. Thus, the recrystallization seen in this work after 2 hours of irradiation at 377 K and 2 hours at 1223 K can be attributed to a combination of a slightly worse contact than expected, resulting in a higher temperature than that predicted through ANSYS  $(\sim +100 \text{ K}, \text{ as higher temperatures would result in melting of the copper disk})$ , combined with an initially heavily damaged (rolled and double forged) state of the sample and the combined simultaneous effect of radiation and thermal loads on the sample, through active annealing during the irradiation.

Hardness measurements performed subsequently using instrumented indentation on a Zwiki ZHU0.2 shows a softening of the sample due to recrystallization. The indentations are carried out using a Vickers indenter to a depth of 15  $\mu$ m at a loading rate of 0.133 N/s and a holding time of 10 seconds at a maximum loading of 15 N force. A pristine sample shows an average indentation hardness of 5.48  $\pm$  0.2 GPa. Similar indentation measurements on the low temperature irradiated sample measures 6.28  $\pm$  0.13 GPa for 0.007 dpa dose, a rise of 0.8  $\pm$  0.4 GPa over unirradiated W, which agrees well with fission irradiation measurements [26]. However, the recrystallized sample displays an indentation hardness of 4.86  $\pm$  0.4 GPa, a drop of 0.6  $\pm$  0.4 GPa, in spite of the 0.006dpa irradiation damage. Similar behaviour has been reported previously on tungsten [33]. This softening is characteristic and agrees with the onset of recrystallization as seen on the sample. Hence it is reasoned that the protons are suitably able to simultaneously subject thermal loads and irradiation damage. Further work to repeat the high-temperature experiment with soldered thermocouple-temperature measurement is foreseen.

IOP Publishing Phys. Scr. 96 (2021) 124014 R Rayaprolu et al

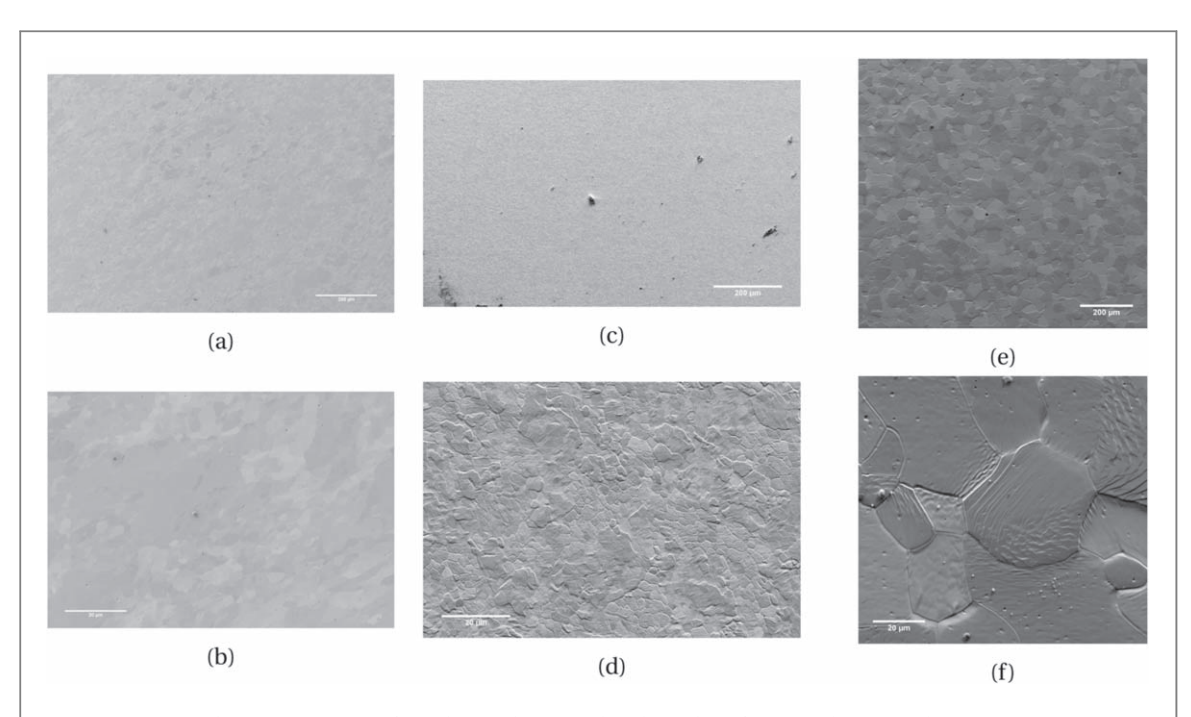


**Figure 6.** Scanning electron microscopy of sample: (a)&(b) un-irradiated sample surface. (c)&(d) post-irradiation copper casing covered sample surface. (e)&(f) 16 MeV proton irradiated 0.006 dpa dose, sample surface (high temperature). The images on top are at  $100 \times$  magnification while the bottom images are taken at  $1000 \times$  magnification.

### 5. Summary

A method to irradiate fusion relevant macroscopic samples with higher energy protons (12-30 MeV) using the linear pre-Bragg region has been designed and tested. It involves sample arrangement and size design and has been used to test W under a low-temperature and high-temperature scenario. The electronic loss from protons results in deposited heat which can be modelled as a heat flux for thin samples. Thus a simultaneous heat load and irradiation damage can be tested using higher energy protons.

Post high-temperature irradiation, the W sample is measured for transmutation under a gamma detector and compares within  $2\times$  of the radiometric modelling. Due to an update in production crosssections for W, further use of TENDL-2017 is recommended against the earlier TENDL-2015. Post high-temperature irradiation, the sample also underwent recrystallization as seen under a scanning electron microscope. Indentation hardness measurements show irradiation hardening of  $0.8\pm0.4$  GPa for low temperature (measured at 373 K) irradiation, while the recrystallized high temperature (estimated at 1223 K) sample showed a softening of  $0.6\pm0.4$  GPa against an unirradiated W sample.

The result indicate pre-deformed state, high temperatures, heat fluxes, and irradiation damage as a combination of factors responsible for the early recrystallization of pure W. Recent fission reactor studies suggest large proportions of Re introduced through transmutation delays the recrystallization of W. As higher energy protons can predict the correct production of Re in W, further experiments to higher heat loads and irradiation doses by increasing the proton current alongside grain growth measurements are essential to study the recrystallization behaviour of W.

#### Data availability statement

The data that support the findings of this study are available upon reasonable request from the authors.

#### References

- $[1]\ Linsmeier\ C\ \emph{et\ al}\ 2017\ Material\ testing\ facilities\ and\ programs\ for\ plasma-facing\ component\ testing\ \emph{Nucl.}\ Fusion\ 57\ 9$
- [2] Federici G, Biel W, Gilbert M, Kemp R, Taylor N and Wenninger R 2017 Nucl. Fusion 57 092002
- [4] Hwang T, Fukuda M, Nogami S, Hasegawa A, Usami H, Yabuuchi K, Ozawa K and Tanigawa H 2016 Nuclear Materials and Energy 9 430–5
- [5] Yi X, Jenkins M L, Hattar K, Edmondson P D and Roberts S G 2015 Acta Mater. 92 163–77
- [6] Armstrong D, Yi X, Marquis E and Roberts S 2013 J. Nucl. Mater. 432 428-36
- [7] Armstrong D, Wilkinson A and Roberts S 2011 Phys. Scr. 2011 014076

- [8] Was GS 2015 J. Mater. Res. 30 1158-82
- [9] Was G S 2016 Simulation of Neutron Irradiation Effects with Ions Fundamentals of Radiation Materials Science: Metals and Alloys (Berlin: Springer)
- [10] Rayaprolu R, Möller S, Abernethy R, Rasinski M, Haley J C and Linsmeier C 2020 Nuclear Materials and Energy 25 100776
- [11] Rayaprolu R, Möller S, Linsmeier C and Spellerberg S 2016 Nuclear Materials and Energy 9 29-35
- [12] Jepeal S J, Snead L and Hartwig Z S 2021 Mater. Des. 200 109445
- [13] Ziegler J F, Ziegler M D and Biersack J P 2010 Nucl. Instrum. Methods Phys. Res., Sect. B 268 1818–23
- [14] Reiser J, Hoffmann J, Jäntsch U, Klimenkov M, Bonk S, Bonnekoh C, Hoffmann A, Mrotzek T and Rieth M 2017 Int. J. Refract. Met. Hard Mater 64 261–78
- [15] Kurishita H et al 2013 Materials Transactions 54 456-65
- [16] Lucas G E 1990 Metallurgical Transactions A 21 1105-19
- [17] Jung P, Hishinuma A, Lucas G E and Ullmaier H 1996 J. Nucl. Mater. 232 186–205
- [18] Lucas GE, Odette GR, Sokolov M, Spätig P, Yamamoto T and Jung P 2002 J. Nucl. Mater. 307-311 1600-8
- [19] Lucas G E, Odette G R, Matsui H, Möslang A, Spätig P, Rensman J and Yamamoto T 2007 J. Nucl. Mater. 367–370 1549–56
- [20] Spellerberg S, Scholten B, Spahn I, Bolten W, Holzgreve M, Coenen H H and Qaim S M 2015 Appl. Radiat. Isot. 104 106-12
- [21] Toda Y, Satoh Y, Kaneda Y, Suzukawa I and Yamada T 1983 IEEE Trans. Nucl. Sci. 30 1405-7
- [22] 2016 ASTM International E521-16: Standard Practice for Investigating the Effects of Neutron Radiation Damage Using Charged-Particle Irradiation. . doi: (https://doi.org/10.1520/E0521-16)
- [23] Stoller R E, Toloczko M B, Was G S, Certain A G, Dwaraknath S and Garner F A 2013 Nucl. Instrum. Methods Phys. Res., Sect. B 310 75–80
- [24] Fukuda M, Kiran Kumar N A P, Koyanagi T, Garrison L M, Snead L L, Katoh Y and Hasegawa A 2016 J. Nucl. Mater. 479 249-54
- [25] Hu X, Koyanagi T, Fukuda M, Kumar N A P K, Snead L L, Wirth B D and Katoh Y 2016 J. Nucl. Mater. 480 235-43
- [26] Katoh Y et al 2019 J. Nucl. Mater. 520 193-207
- [27] Garrison L M, Katoh Y and Kumar N A P K 2019 J. Nucl. Mater. 518 208-25
- [28] Goorley J T, James M R, Booth T E, Brown F B, Bull J S, Cox L J, Durkee Jr J W and Elson J S 2013 Initial mcnp6 release overview-mcnp6 version 1.0 Report Los Alamos National Lab. (LANL) Los Alamos, NM (United States)
- [29] Sublet J C, Eastwood J, Morgan J, Gilbert M, Fleming M and Arter W 2017 Nucl. Data Sheets 139 77-137
- [30] Koning A J and Rochman D 2012 Nucl. Data Sheets 113 2841-934
- [31] Pintsuk G, Bobin-Vastra I, Constans S, Gavila P, Rödig M and Riccardi B 2013 Fusion Eng. Des. 88 1858-61
- [32] Miyazawa T, Garrison L M, Geringer J W, Echols J R, Fukuda M, Katoh Y, Hinoki T and Hasegawa A 2020 Tensile properties of powder-metallurgical-processed tungsten alloys after neutron irradiation near recrystallization temperatures J. Nucl. Mater. 542
- [33] Mathaudhu S N, deRosset A J, Hartwig K T and Kecskes L J 2009 Materials Science and Engineering: A 503 28-31